Infection dynamics and virulence potential of clinical *Pseudomonas aeruginosa* isolates in human airway epithelial models

Claudia Antonella Colque[1,#,*], Signe Lolle[1,#], Ruggero La Rosa[1,*], Maria Pals Bendixen[1], Asha M. Rudjord-Levann[1], Filipa Bica Simões[1], Kasper Aanæs[2,3], Søren Molin[4], Helle Krogh Johansen[1,2*].

[1] Department of Clinical Microbiology 9301, Rigshospitalet, 2100 Copenhagen Ø, Denmark

[2] Department of Clinical Medicine, Faculty of Health and Medical Sciences, University of Copenhagen, 2200 Copenhagen, Denmark.

[3] Department of Otorhinolaryngology, Head and Neck Surgery & Audiology, Rigshospitalet, 2100 Copenhagen Ø, Denmark.

[4] The Novo Nordisk Foundation Center for Biosustainability, Technical University of Denmark, 2800 Kgs. Lyngby, Denmark.

# These authors contributed equally.

* Corresponding authors: Claudia Antonella Colque (antcol@biosustain.dtu.dk), Ruggero La Rosa (rugros@dtu.dk), Helle Krogh Johansen (hkj@biosustain.dtu.dk).

Short Title: *P. aeruginosa* infections in ALI models

Abstract

Persistent bacterial infections constitute an increasing health problem, often associated with antibiotic resistance. However, despite extensive antibiotic treatment, *Pseudomonas aeruginosa* persists for decades in people with cystic fibrosis (pwCF), remaining susceptible. Host-pathogen interactions during infection may, therefore, be a major contributing factor to treatment failure. Using an infection model based on human airway epithelial cells, cultured at the air-liquid interface (ALI), we simulated the infection process of *P. aeruginosa* to investigate the colonization dynamics and virulence potential during infection in ALI models from non-CF and CF donors, and the BCi-NS1.1 cell line. Infections by reference strains and clinical isolates from pwCF revealed four infection clusters based on virulence, epithelial damage, and localization within the epithelium, in a strain-specific manner regardless of the type of ALI model or clonal lineage. Modulator treatment to restore CFTR channel function did not change infection patterns in CF ALI models. Dual RNA-seq revealed that bacterial colonization of ALI models significantly upregulated host inflammatory pathways, dependent on the strain's virulence. Simultaneously, while bacterial gene expression was similar in non-CF and BCi-NS1.1 ALI models, CF models promoted differential regulation in a type III secretion mutant. Altogether, our results profile key infection dynamics occurring in pwCF and provide ground knowledge on the interplay between the airway epithelium and *P. aeruginosa*.

52 **Introduction**

53 With increasing lifespans and changes in lifestyle, persistent bacterial infections are on the
54 rise (*1*). Although antibiotics are generally effective, diagnosing and treating these infections
55 is often challenging because of their complexity and the continuous changes in both the host
56 and pathogen (*2*). This is worsened by the lack of robust and reliable model systems to predict
57 infection outcomes and treatment efficacy. However, by understanding treatment failures in
58 physiologically relevant model systems, improved diagnostics and therapies can be developed
59 (*3*).

60 People with cystic fibrosis (pwCF) often suffer from persistent bacterial infections
61 caused by a plethora of bacterial pathogens that colonize the airways and persist for decades.
62 Cystic fibrosis (CF) is caused by mutations in the cystic fibrosis transmembrane conductance
63 regulator protein (CFTR), which is crucial for fluid homeostasis (*4*). CFTR mutations result in
64 impaired chloride secretion, increased mucus viscosity and reduced cilia beating, ultimately
65 leading to reduced mucociliary clearance (*5*). This creates the perfect environment for
66 pathogenic bacteria, such as *Pseudomonas aeruginosa*, which is the leading cause of
67 respiratory morbidity and mortality in pwCF (*6*, *7*). Recent advances in CFTR modulator
68 therapies, particularly elexacaftor/tezacaftor/ivacaftor (ETI), significantly improve the well-
69 being in pwCF by correcting and potentiating the function of the CFTR channels (*8*). While it
70 has been shown that during ETI treatment bacterial pathogen counts decrease (*9*), *P.*
71 *aeruginosa* often persists indicating the need for a deeper understanding of the relationship
72 between ETI treatment and *P. aeruginosa* infections in pwCF (*10*–*12*).

73 Early infections are caused by environmental *P. aeruginosa* strains which adapt, over
74 the years, to the CF host environment through genetic, metabolic, and phenotypic changes
75 (*13*, *14*). This enhances antibiotic resistance, immune escape, a biofilm lifestyle and reduces
76 virulence factor production (*15*–*18*). In most patients, the initial clone drives within-host
77 adaptation. Person-to-person transmission has also been documented in pwCF, and especially
78 *P. aeruginosa* clones such as the DK01 and DK02 (Denmark), and high-frequent clones such as
79 the C clone (ST17 clone, present in Europe and North America and persistent in pwCF) and
80 PA14 (ST253 clone, found worldwide with affinity to CF and non-CF infections) have this
81 capability (*19*–*25*). However, how colonization and infection dynamics evolve during infection
82 from a *P. aeruginosa*-human airway point of view remains largely unclear. This includes 1) the
83 role of virulence factors, toxins, and specific dominant strains in tissue invasion and immune

84 escape, 2) the epithelial response and long-term effects on epithelial integrity and function,
85 and 3) how modulator treatment changes the infection pattern and the interaction between
86 the airway epithelium and the pathogen. Understanding the early stages of colonization,
87 therefore, may shed light on the bacterial pathogenic potential, antibiotic treatment failure,
88 and allow exploration of new treatment options. In addition, lack of reliable *in vitro* models
89 which recreate the microenvironment for studying infection processes in the airway limits our
90 understanding of colonization dynamics and bacterial virulence potential within human
91 tissues (*26*).

92 Host-pathogen interactions in the human airways have traditionally been investigated
93 in monolayer cell cultures, most of which are based on cancer cell lines, primary cells or tissue
94 explants (*27*). These present high genomic instability, challenges for their isolation and
95 maintenance, and lack the spatial context required to accurately mimic the cellular and
96 molecular markup of human airway epithelium. To overcome these limitations, we employed
97 3D air-liquid interface (ALI) models based on the BCi-NS1.1 cell line and primary cells from CF
98 and non-CF donors, which closely mimic the human airway epithelium, exhibiting
99 differentiation, cell polarization, mucus production, and ciliary beating, which are
100 fundamental parameters in understanding infection dynamics and colonization processes (*28*,
101 *29*).

102 Recent studies have used ALI systems to shed light on *P. aeruginosa* infection
103 processes, resistance mechanisms, and metabolic adaptation (*30*–*37*). Specifically, infection
104 dynamics and localization of the bacteria within the epithelium can influence both host
105 response and antibiotic susceptibility/resistance (*38*). Similarly, bacterial metabolic processes
106 can influence the host immune response (*17*). However, these studies used laboratory strains
107 which do not reflect the complexity of clinical CF isolates and their infection dynamics.
108 Therefore, modeling infection patterns in physiologically relevant models with clinically
109 relevant strains is of high priority to understand treatment failure and overcome bacterial
110 persistence (*3*).

111 In this study, we used ALI models to profile *P. aeruginosa* infection using 12 clinical
112 strains isolated from pwCF from frequent and distinct lineages and compared them with well-
113 characterized reference strains. We determined the overall host response to the bacterial
114 infections, including epithelial integrity, cytotoxicity, cytokine secretion, and bacterial
115 colonization patterns in *P. aeruginosa*-infected ALI models generated with non-CF or CF

116 primary cells, or the human telomerase reverse transcriptase (hTERT) immortalized airway
117 basal cell line BCi-NS1.1. Additionally, we determined the impact of the CFTR modulator ETI
118 on *P. aeruginosa* infection pattern. Dual RNA-seq analysis unfolded host-pathogen interactions
119 at the molecular level. Our results highlight the importance of host-pathogen model systems
120 to understand infection dynamics and promote the development of new therapies.
121
122 **Results**
123 *Host response upon bacterial infections in ALI models*
124 To study the early dynamics of epithelial colonization, and to determine whether non-CF and
125 CF-derived epithelial tissues elicit individual responses upon *P. aeruginosa* infections, we
126 performed bacterial infection assays using airway ALI models (Fig S1). These recapitulate the
127 human lung epithelium, and are state-of-the-art within human airway infection models (*28*,
128 *31*, *33*). Specifically, we evaluated infection capabilities and epithelial response, in ALI models
129 generated with: 1) primary basal cells from non-CF (n = 3) or pwCF (n = 7) donors, and 2) the
130 hTERT-immortalized basal airway cell line BCi-NS1.1 (*39*) (Fig S1). For each infection, we
131 quantified epithelial response and bacterial proliferation by measuring: 1) the transepithelial
132 electrical resistance (TEER) to quantify the integrity of the epithelial barrier, 2) the release of
133 lactate dehydrogenase (LDH) to quantify the induced epithelial cell lysis, 3) the secretion of
134 the chemokine Interleukin-8 (IL-8) to quantify the onset of inflammation, and 4) the bacterial
135 colony-forming units (CFU) to quantify the bacterial load post-infection. Infections were
136 carried out using a collection of early (*_E), intermediate (*_I), and late (*_L) *P. aeruginosa*
137 clinical isolates from pwCF belonging to distinct clone types (lineages which differ by >10,000
138 SNPs), which comprise different stages of CF adaptation, evolutionary histories and infection
139 scenarios (Table S1) (*40*, *41*). These clone types were chosen based on their frequency in the
140 Copenhagen CF Clinic (DK01 and DK02) and worldwide (C and PA14 clone, DK06 and DK19
141 clones in Denmark, respectively). In addition, we included well-characterized *P. aeruginosa*
142 reference strains (PAO1 and PA14), including a PAO1 derivative lacking the virulence
143 determinant *pscC* of the Type III secretion system (T3SS). The T3SS plays an important role in
144 the transition from acute to chronic/persistent infection occurring during host adaptive
145 evolution (*42*, *43*). Additionally, it is involved in host colonization, invasion and cell damage,
146 as we, and others have previously reported (*17*, *33*, *34*). The chosen bacterial strains exhibit
147 distinct phenotypes characterized by both high and low growth rates, motility, and mild-to-

high increased minimum inhibitory concentration (MIC) to tobramycin, ciprofloxacin, and ceftazidime (Fig S2). These strains are representative of the heterogeneity of *P. aeruginosa* infecting population present in pwCF (*44–46*). To ensure a comparable bacterial load post-infection across all samples, fast growing strains were incubated in ALI models for 14 h while slow growing strains were incubated for 38 h (Fig S3). Consistent with this experimental set-up, no significant differences in CFUs were observed across bacterial strains and ALI models (Kruskal-Wallis followed by Dunn's post-hoc test, $p>0.05$) (Fig S3). Additionally, Pearson correlation analysis showed no correlation between the total CFU relative to TEER (r=-0.27, p=0.001), LDH release (r=-0.004, p=0.9601), or IL-8 secretion (r=0.12, p=0.1441), indicating independence of the variables. In addition, strain-specific bacterial infection outcomes (TEER, CFU, LDH, and IL-8) were overall comparable across non-CF, CF, and BCi-NS1.1 ALI models (Kruskal-Wallis followed by Dunn's post-hoc test, $p>0.05$), except for DK01_L, DK06_L and DK19_L infections, where LDH release was significantly higher in CF compared to non-CF and BCi-NS1.1 ALI models (Kruskal-Wallis followed by Dunn's post-hoc test, $p<0.01$, Table S2: Infection Dynamics). In all cases, Pearson correlation analysis of infection data across the different ALI models showed values > 0.9 ($p<0.001$) (Fig 1A). This suggests that in our model system, the infection outcomes (TEER, CFU, LDH, and IL-8) are mostly dependent on the specific virulence potential of the infecting bacteria rather than on the different ALI models (non-CF, CF, or BCi-NS1.1). All infection data are detailed in Table S2: Infection dynamics.

When comparing across all infections (ALI, n = 194), TEER measurements pre-infection revealed tissue dependent values, with BCi-NS1.1 models exhibiting the highest TEER followed by CF and non-CF ALI models (Kruskal-Wallis followed by Dunn's post-hoc test, $p<0.0001$) (Fig 1B). Similarly, CF models exhibited the highest level of cellular damage (LDH release) and highest inflammatory response (IL-8 secretion) (Kruskal-Wallis followed by Dunn's post-hoc test, $p<0.01$) (Fig 1C, D). Comparable results were obtained when discriminating by the duration of infection (14 h vs 38 h) and mock infected ALI models (Fig S4). Moreover, CF ALI models exhibited a time-dependent increase of LDH release (Kruskal-Wallis followed by Dunn's post-hoc test, $p<0.01$) (Fig S4D).

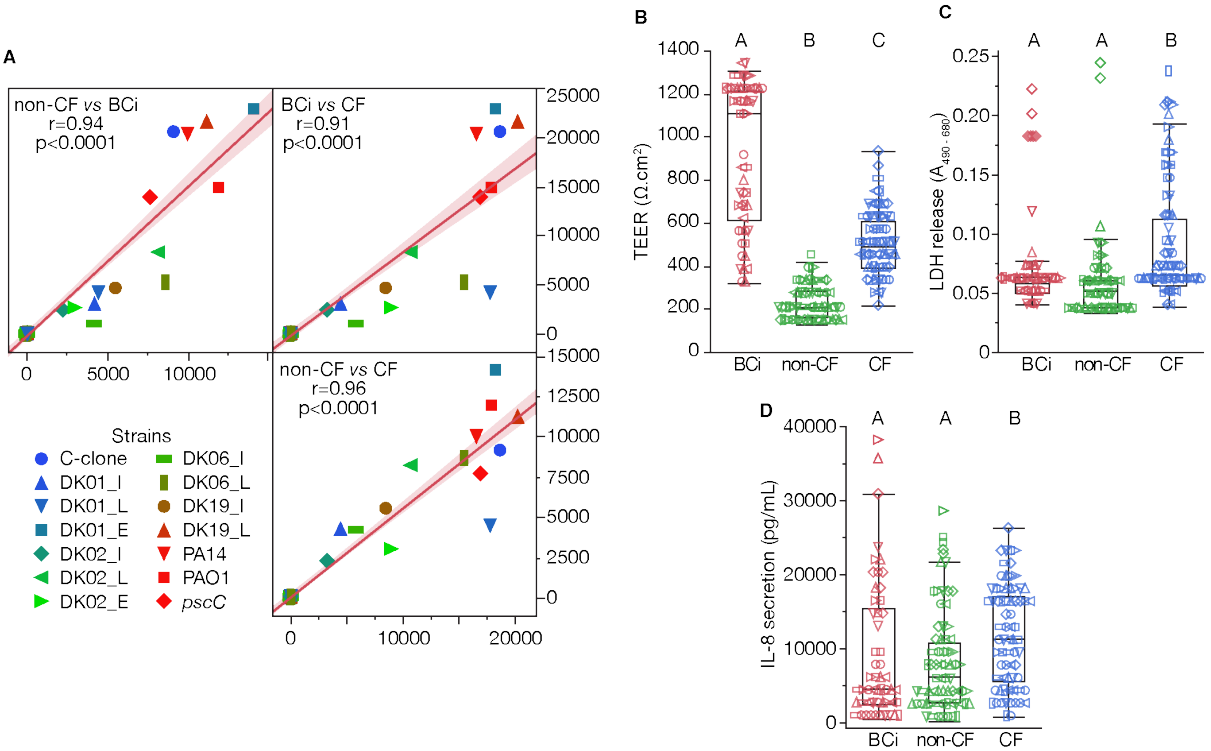

Fig 1. Infection outcomes across ALI models and bacterial strains. A) Pearson correlation analysis of the infection data across ALI models and bacterial strains. Pearson's correlation coefficient r, statistical significance (p value), linear fitting between the variables, and 95 % confidence interval are indicated in the graph. B) TEER measurements of non-CF, CF, and BCi-NS1.1 ALI models after 28 days of differentiation in the absence of bacterial infections. Quantification of C) LDH release and D) IL-8 secretion by non-CF, CF, and BCi-NS1.1 models 14 h or 38 h post infection. Infections were carried out for 14 h for early and intermediate strains (DK01, DK02, DK06 and DK19) and laboratory strains (PAO1 and PA14) and for 38 h for late strains (DK01, DK02, DK06 and DK19). In B, C and D, statistical significance was computed by Kruskal-Wallis followed by Dunn's post-hoc test, where connecting letters report significance between groups ($p<0.05$). CF: cystic fibrosis; BCi: BCi-NS1.1; TEER: transepithelial electrical resistance; LDH: lactate dehydrogenase; IL-8: Interleukin-8.

The recent development of CFTR modulator treatment has changed the clinical approach to CF treatment. However, several reports indicate the persistence of *P. aeruginosa* within the airway of ETI treated pwCF (*10*, *12*), suggesting that restoration of airway epithelial functionality is not enough for pathogen eradication. For this reason, we tested *P. aeruginosa*

197 infection capacity in ETI-treated and untreated CF ALI models. First, we confirmed the effect
198 of ETI in CF ALI models (n = 3, donors homozygous for ΔF508) in the absence of *P. aeruginosa*.
199 A significant decrease in TEER and an increase in transepithelial electrical conductance (TEEC),
200 an indirect parameter of CFTR function (*47–49*), was observed in CF ALI models after 24 h of
201 ETI treatment (Fig 2A, B). Contrary, no effect was observed in non-CF cells irrespective of ETI
202 treatment (Fig S5A, B). Increased CFTR protein expression at the apical membrane was
203 confirmed by immunofluorescent staining of ETI-treated CF ALI models (Fig 2C). Having
204 confirmed restoration of CFTR function and localization, we next evaluated whether ETI
205 treatment altered the infection capacity of *P. aeruginosa* in non-CF and CF ALI models (Table
206 S2: ETI treatment). Infection outcomes in ETI-treated and untreated ALI models using PAO1
207 (Fig 2D, E) and the clinical strains DK01_I and DK02_L (Fig S5C, D) showed no difference in
208 TEER, CFU, or bacterial distribution within the CF ALI models. A similar response was observed
209 when the same strains infected non-CF ALI models (Fig S5E, F).
210 Despite intrinsic differences between non-CF, CF, and BCi-NS1.1 ALI models, our results
211 suggest that infection dynamics are independent of the ALI type or modulator treatment and
212 may depend on the bacterial lineage or other factors not recreated in the ALI model.
213

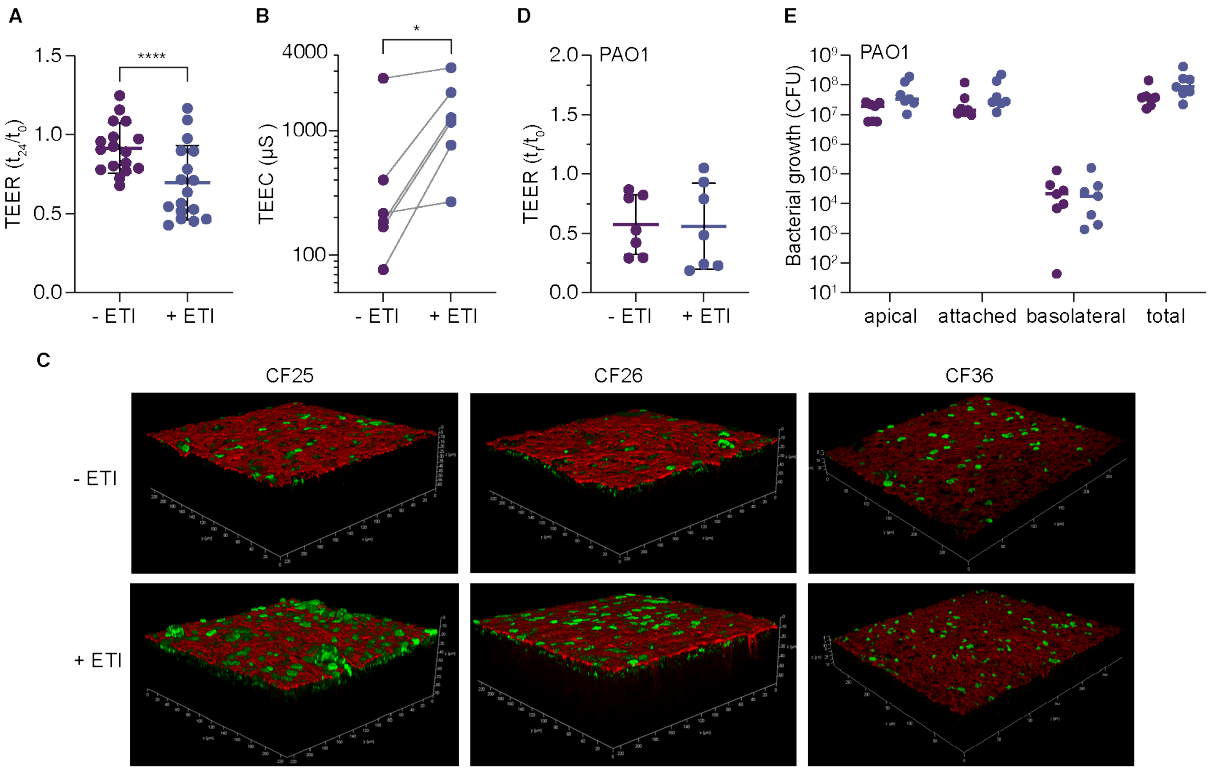

214
215

Fig 2. Effect of elexacaftor/tezacaftor/ivacaftor (ETI) on cystic fibrosis (CF) ALI models infected with PAO1. A) TEER fold change in CF ALI models treated ± ETI for 24 h. B) TEEC after CFTR stimulation in ALI models treated ± ETI. Each data point represents one independent donor. C) Three-dimensional reconstruction of confocal microscopy images of immunofluorescent staining of CFTR protein in ALI models from the CF donors ± ETI. Green: Anti-CFTR 570 (CFTR protein), Red: Phalloidin (F-actin). D) TEER change after 14 h of infection with PAO1 laboratory strain ± ETI. E) Bacterial growth (CFU) after 14 h of infection in the apical (non-attached / free bacteria), attached to the epithelium, and basolateral compartment, along with the total number of bacteria. In A, C and D, each data point represents one independent experiment, and the mean ± SD is included. Statistical significance was calculated by paired two-sided t-test where **$p<0.01$ and ****$p<0.0001$. ALI: air-liquid interface; TEER: transepithelial electrical resistance; TEEC: transepithelial electrical conductance; CFU: colony-forming units.

Strain-specific infection phenotypes of P. aeruginosa

After years of adaptive evolution in pwCF, *P. aeruginosa* changes its phenotype in response to stresses such as antibiotics, reactive oxygen species (ROS), immune cells and others (*24*, *50*). Therefore, we next evaluated whether differences in strain adaptive evolution and historical contingency affected the infection capabilities in a convergent manner. Given that bacterial infections progressed similarly across the different ALI models and independent of ETI treatment, for each strain, we averaged the infection data from non-CF, CF, and BCi-NS1.1 ALI models (Table S2: Infection Dynamics Median.).

PCA and K-Means clustering identified four clusters of strains with similar infection properties which can be associated primarily with their virulence, epithelial damage, and localization within the epithelium (Fig 3A). PC 1 (44.8 % of the variance) clusters strains based on their virulence potential with cluster 1 and 2 showing a decrease in TEER, and an increase in cytotoxicity (LDH release), and inflammatory response (IL-8) (Fig 3A, B). Contrary, PC 2 (36.2 % of the variance) separates strains based on their ability to penetrate the epithelium. Strains from cluster 1 are found in the basolateral compartment, indicating increased penetration through the epithelium, while strains from cluster 3 are found predominantly attached within the epithelium (Fig 3A, B). It is worth noting that while the *pscC* mutant strain, and the DK02_L

248 isolate, group in the more virulent cluster 1 and 2, respectively, both strains show
249 intermediate infection capabilities comparable with strains from cluster 3 and 4 (Fig 3B).
250 Interestingly, while virulent strains from cluster 1 and 2 colonized the epithelia as large
251 aggregates/biofilm structures, less virulent strains from cluster 3 and 4 infected as single
252 colonies or small bacterial aggregates, as shown by confocal microscopy (Fig 3C and Fig S6).
253 Furthermore, most virulent strains (PAO1, PA14, and DK02_L) and a few low virulent strains
254 (*pscC* mutant strain and DK06_L isolate) caused cell shedding. Lastly, variations in colonization
255 pattern were observed within each cluster. For instance, from cluster 2, only PA14 was found
256 within the epithelium, whereas DK01_E was found overlapping with mucus-producing cells.
257 The latter was also seen for DK01_I and DK02_I from cluster 4 (Fig 3C, Fig S6).

258

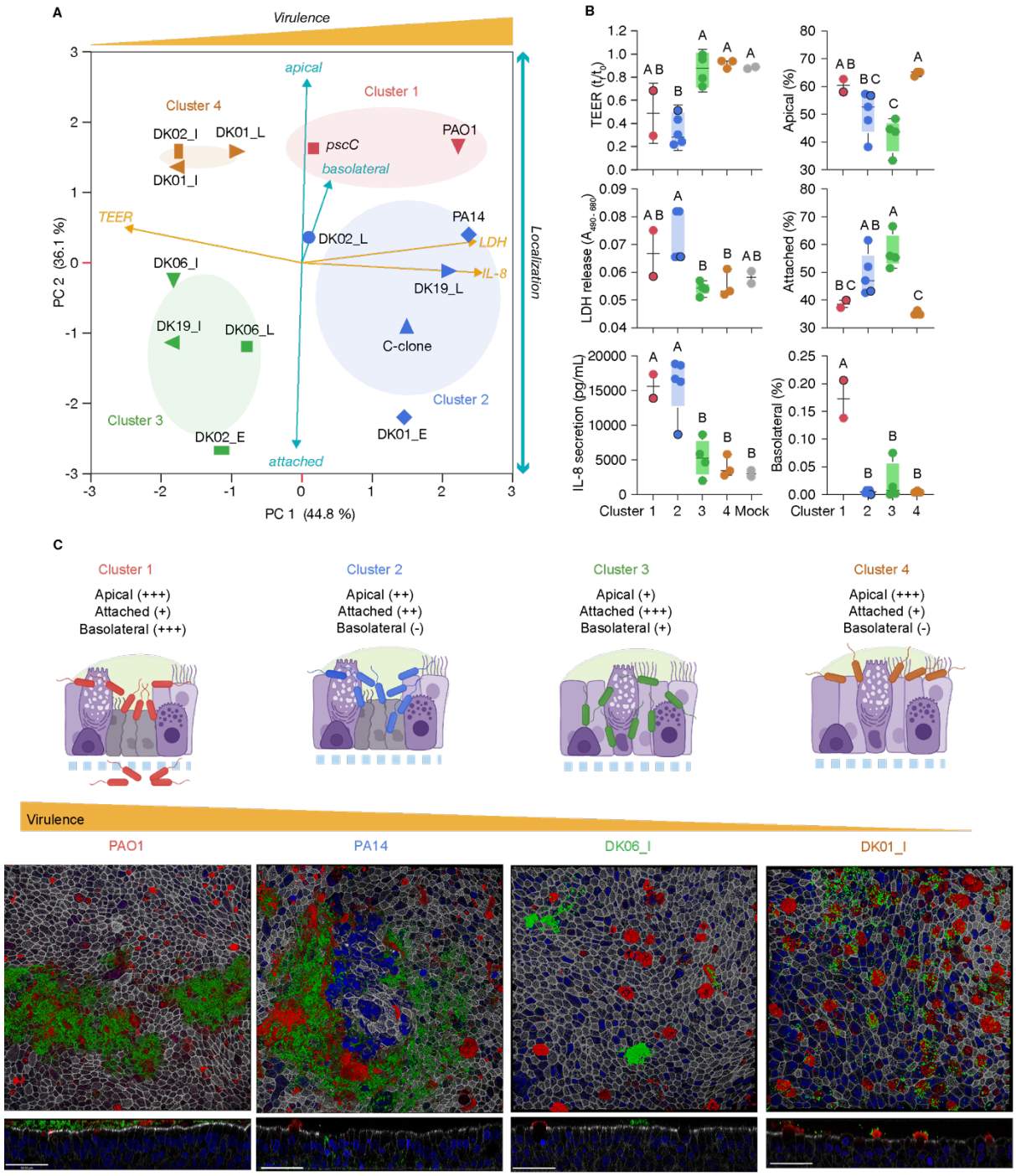

259

260 **Fig 3. Infection phenotypes of *Pseudomonas aeruginosa* strains.** A) PCA and K-mean
261 clustering of the infection phenotypes of laboratory (PAO1, *pscC* mutant strain, PA14, and C-
262 clone) and clinical strains (early, intermediate, and late DK01, DK02, DK06, and DK19) of *P.*
263 *aeruginosa.* Each symbol represents the median infection phenotypes in non-CF, CF, and BCi-
264 NS1.1 ALI models explained by the variables TEER, LDH release, IL-8 secretion, and distribution

of bacteria in the apical, attached, and basolateral compartment. K-mean clusters (1 to 4) and PCA loadings are color-coded to underline groupings of strains and explained variance, respectively. B) Box plot of the specific K-mean clusters characteristics for TEER, LDH release, IL-8 secretion, and normalized distribution of CFUs in the apical, attached, and basolateral compartment. The outlined symbols in clusters 1 and 2 represent *pscC* mutant strain and DK02_L strains, respectively. Statistical significance was computed by Kruskal-Wallis followed by Dunn's post-hoc test, connecting letters report significance between groups ($p<0.05$). C) Colonization phenotype of strain-specific clusters in CF cells. Schematic representation of CF ALI models (purple) challenged with strains from clusters 1 (red), 2 (blue), 3 (green), and 4 (brown). Representative confocal microscopy images of CF ALI models infected with strains from Cluster 1 (PAO1), Cluster 2 (PA14), Cluster 3 (DK06_I) and Cluster 4 (DK01_I). Top and cross-sectional views of ALI models are shown. Representative images from all strains infecting CF ALI models are shown in Fig S6. Immunofluorescent staining: sGFP (green) staining chromosomally tagged bacteria; MUC5AC (red) specific for mucus producing cells; Phalloidin (white) specific for actin, and DAPI (blue) nuclear stain. Stainings were done in three biological replicates, one representative image is shown for each infection. PCA: principal component analysis; TEER: transepithelial electrical resistance; LDH: lactate dehydrogenase; IL-8: Interleukin 8.

Dual RNA-sequencing of host and pathogen in P. aeruginosa*-infected ALI models*

While different bacterial strains showed similar infection patterns across all ALI models, the molecular response of both bacteria and host is likely influenced by the specific comparisons (*i.e.*, non-CF, CF, or BCi-NS1.1 ALI models and different *P. aeruginosa* strains). To test this hypothesis, we performed dual RNA-seq analysis of ALI models from the BCi-NS1.1 cell line, a non-CF donor, and a CF, with PAO1, *pscC* mutant strain and mock infected (Fig 4A, Table S2: RNAseq). This approach allowed us to analyze the molecular responses of isogenic bacteria, while capturing differences in the colonization process of highly virulent and intermediate virulent-like clinical strains, represented by the PAO1 and *pscC* mutant strain, respectively (Fig 3A). While it is known that the T3SS is crucial in host colonization and invasion (*33*), its role at the molecular level during host interactions remains unknown.

296 PCA analysis of the host response (n = 18746 genes) showed that: 1) the transcriptional
297 program of infected ALI models (PAO1 and *pscC* mutant strain) differed from mock infected
298 (mock) (Fig 4B), and 2) that primary cells, *i.e.*, non-CF and CF ALI models, exhibited a different
299 host response relative to BCi-NS1.1 models (Fig 4B). Pearson correlation analysis of gene
300 expression (n = 18746) in mock infected non-CF, CF, and BCi-NS1.1 ALI models, was positive
301 and significant (Pearson's $r>0.97$; $p<2.2e^{-16}$), thus ensuring that any intrinsic variability
302 between the different models would not significantly impact the downstream differential
303 expression analysis (Fig S7A). A similar trend was found in mock infected samples, when only
304 analysing the 455 differentially expressed genes (DEGs) found in the comparison PAO1 vs
305 mock (Pearson's $r>0.94$; $p<2.2e^{-16}$) (Fig S7B), indicating that the different ALI models do not
306 have functional impact on gene regulation post infection. IL-8 secretion and CXCL8 gene
307 expression, responsible for IL-8 protein expression, was positively correlated (Pearson's $r =$
308 0.9891; $p<0.0001$) confirming higher levels of chemokine secretion in infected samples
309 compared to mock infected samples, thus validating our RNA-seq data (Fig 4C).
310 Analysis of bacterial expression profiles (n = 4255 genes) revealed: 1) bacteria infecting
311 non-CF and BCi-NS1.1 ALI models behave similarly, 2) infection in CF models drives a distinct
312 bacterial expression profile, and 3) differences dependent on the bacterial genetic background
313 (Fig 4D).
314

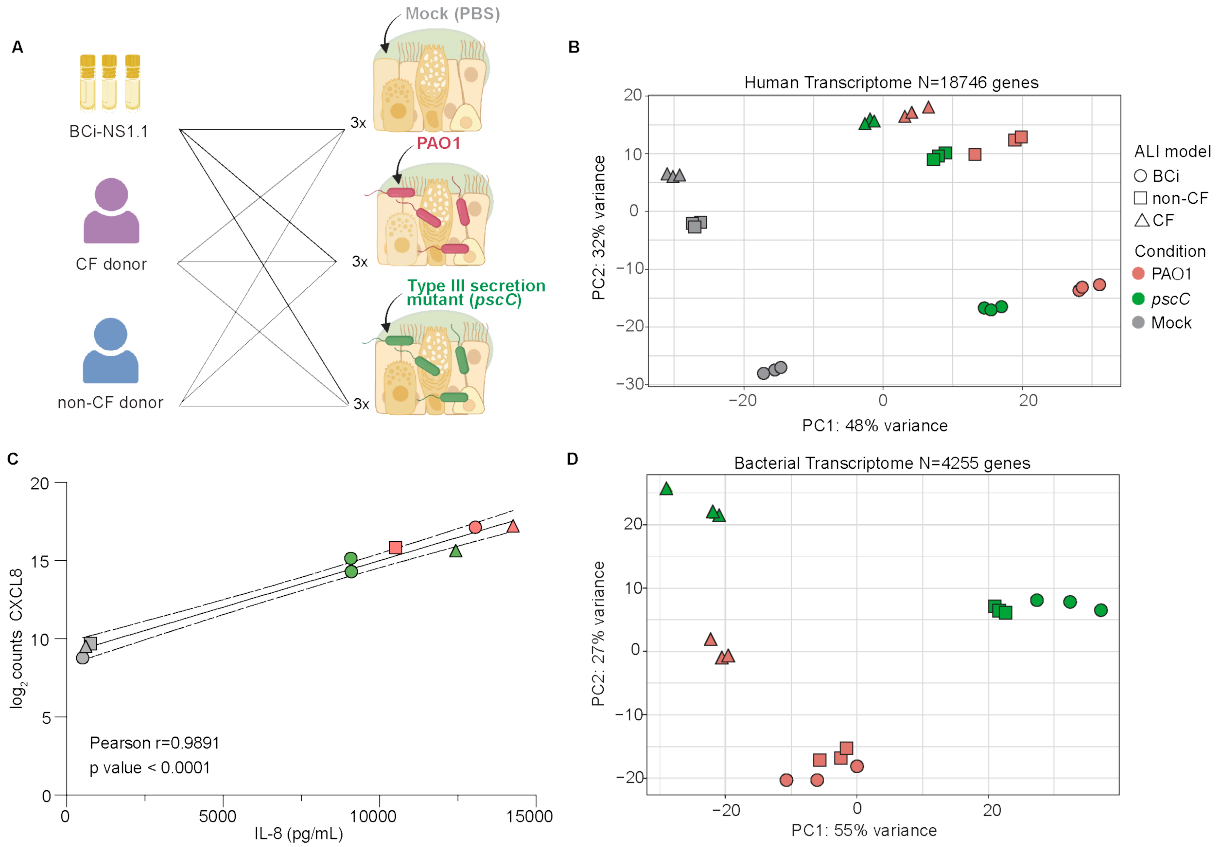

Fig 4. Exploring the transcriptional responses from human and pathogen upon infection. A) Schematic representation of the ALI models (non-CF, blue; CF, purple; BCi-NS1.1, yellow) and bacteria (PAO1, red; *pscC* mutant strain, green) used to perform infections and subsequent dual-RNAseq. PCA of $\log_2$ read counts from B) the host and D) the pathogen. Data include the reads of 18746 genes from the human transcriptome and 4255 from the *Pseudomonas aeruginosa* transcriptome, from which differential gene expression analysis was performed. The type of ALI model is presented by symbol shapes: BCi-NS1.1 (circle), CF (triangle), and non-CF (square). Mock infected samples are colored in grey, whereas ALI models infected with PAO1 or *pscC* mutant strain are shown in red and green, respectively. Each data point represents one biological replicate. C) Regression lines and Pearson's correlation coefficient for IL-8 quantification and CXCL8 gene expression ($\log_2$ read counts). 95 % confidence interval lines for the linear regression fit are included. ALI: air-liquid interface; CF: cystic fibrosis; PCA: Principal component analysis; TEER: transepithelial electrical resistance; IL-8: Interleukin-8.

Cellular and inflammatory response in ALI models upon infection with PAO1 and pscC *mutant strain*

333 To characterize the molecular basis of the host response to either PAO1 or *pscC* mutant strain,
334 we performed individual DEG comparisons between ALI models infected with A) PAO1 and
335 mock (Fig 5A), and B) PAO1 and *pscC* mutant strain (Fig 5D). For each comparison, we first
336 compared gene convergence/divergence across the different cell types and second, we
337 performed gene set enrichment analysis using both KEGG and the MSigDB (GO) database.
338 Compared to mock, CF ALI models showed the fewest DEGs, followed by non-CF and
339 BCi-NS1.1 ALI models, when infected with PAO1. For all non-CF, CF, and BCi-NS1.1 infections,
340 we observed mainly upregulated genes (Fig 5B, Table S3). Enrichment analysis showed that *P.*
341 *aeruginosa* triggered upregulation of several pathways related to inflammation via nuclear
342 factor-kappa B (NF-κβ) and tumor necrosis factor alpha (TNFα) and overexpression of
343 cytokines, including IL-6 and IL-17 (Table S4). Of note, colony-stimulating factor (CSF3) and
344 pro-inflammatory cytokine IL17C were among the most DEGs across all types of ALI models
345 (mean $\log_2$ FoldChange = 12.01 ± 1.5 and 11.8 ± 0.6, respectively) (Fig 5C). Other highly
346 expressed genes included chemokine ligand 20 (CCL20) and TNFα, Toll-like Receptor (TLR)-2,
347 TLR4 (involved in recognition of bacterial pili and LPS), IL1B, IL6, CXCL8 (involved in the first
348 stages of infection) and the antimicrobial human beta-defensin 4 (DEF4BA) (Fig 5C).
349 We found subtle differences in host response following infection with the less virulent
350 *pscC* mutant strain, compared to PAO1 (Fig 5E). In fact, only 65 unique genes were
351 differentially expressed in ALI models infected with PAO1 relative to *pscC* mutant strain (Fig
352 5E). Pathways related to cytokine signaling and inflammation were overrepresented among
353 this set of genes, which were primarily highly expressed in PAO1-infected non-CF and BCi-
354 NS1.1 ALI models (Fig 5F). This suggests that, at the time tested, the delivery of effectors from
355 the T3SS partially affects host gene expression. However, *P. aeruginosa* has a wide array of
356 other virulence factors contributing to infection and concomitant inflammatory response,
357 possibly explaining the subtle difference observed between the PAO1 and *pscC* mutant strain.

358

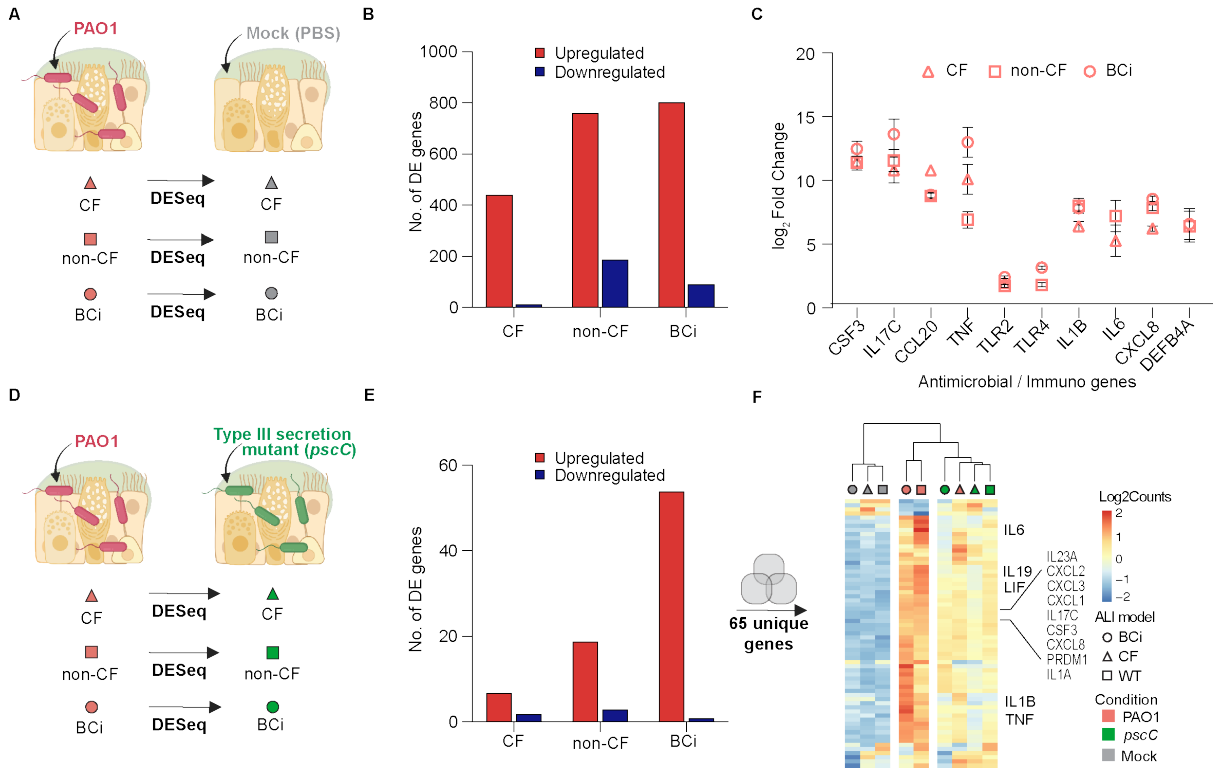

359 **Fig 5. Intrinsic host response before and after colonization with PAO1 and *pscC*.** A)
360 Representation of the individual differential expression comparisons between ALI models
361 were performed: PAO1 and mock infected ALI models. B) Number of differentially expressed
362 genes (DEGs) shown as upregulated (red) and downregulated (blue). An adj p value < 0.05 and
363 $\log_2$ Fold Change ≥ $|1|$ was used as cutoff C) $\log_2$ Fold Change of immune genes when
364 comparing PAO1 infected and mock. Only significantly expressed DEGs are shown. D)
365 Representation of the DEG comparisons between PAO1-infected and *pscC* mutant strain-
366 infected ALI models. E) Number of DEGs shown as upregulated (red) and downregulated
367 (blue). F) Heatmap of $\log_2$ read counts scaled for each gene (row) from the unique 65 DEGs
368 from D) Each column represents the mean of the three biological replicates sequenced
369 clustered based on the result of pvclust analysis. CF: cystic fibrosis; BCi: BCi-NS1.1.

370

371

372 *PAO1 and* pscC *mutant strains elicit differential response upon interaction with ALI models*
373 Analysis of the bacterial transcriptome aimed to evaluate how the expression profile of PAO1
374 and *pscC* mutant strain vary upon interaction with different ALI models (Fig 6A). As previously
375 shown (Fig 4C), whole-gene expression profiling of both bacterial strains was similar in non-
376 CF and BCi-NS1.1 ALI models. Indeed, no PAO1 gene was differentially expressed when

377 comparing non-CF vs BCi-NS1.1 infections, and a similar observation was made for *pscC*
378 mutant strain with only three DEGs (Fig 6B top and bottom panel, Table S5). The PAO1
379 transcriptome (n = 4255 genes) showed only 56 and 79 DEGs in CF vs non-CF and CF vs BCi-
380 NS1.1 infections, respectively, suggesting that PAO1 behaves similarly when colonizing
381 different ALI models (Fig 6B). Contrary, *pscC* mutant strain showed a 3.9-fold and 5-fold
382 increase in DEGs, in CF vs non-CF, and CF vs BCi-NS1.1 infections, respectively (Fig 6B, bottom
383 panel). This suggests that the activity of T3SS has a direct impact on the bacterial expression
384 profile upon infection in CF ALI models.

385 Considering similarities between bacterial gene expression in non-CF and BCi-NS1.1
386 ALI models, we next compared the expression profiles of *pscC* mutant strain and PAO1,
387 focusing on CF and non-CF infections (Fig 6B underlined boxes). Compared with PAO1, an
388 increased number of genes was regulated in the *pscC* mutant strain upon infection in CF ALI
389 models (PAO1 n = 55, *pscC* mutant strain = 218) (Fig 6B). A total of 41 genes were common
390 and included upregulation of genes involved in respiration under iron-limiting conditions such
391 as 1) bo_3 quinol oxidase (*cyo*) genes and 2) members of the *fumC-sodM* iron-responsive
392 operon (Table S6). Likewise, downregulation of several pathways involved in virulence, such
393 as the production and transport of phenazines (among others: *phz1* and *phz2* operons),
394 nitrate reductase *nirA,* and fucose-specific lectin *lecB* was seen in both strains (*53–55*).

395 When comparing the infection of *pscC* mutant strain in CF vs non-CF ALI infections, we
396 found enrichment of three main categories of upregulated genes: 1) iron chelation (related to
397 heme uptake, pyoverdine, and pyochelin transport), 2) sulfate metabolism (*cysAWT-sbp*
398 operon) and, 3) lipid A modifications (Fig 6C, left panel and Table S6). Contrary, several genes
399 related to virulence, including QS and biofilm pathways, were enriched in the downregulated
400 class (Fig 6C, right panel, and Table S6). For example, 1) genes from the *pseudomonas*
401 quinolone signal (PQS) cluster, 2) rhamnolipids coding genes, 3) the type 6 secretion system
402 H2 gene cluster (H2-T6SS), 4) genes from oxide-sensing mechanisms and, 5) elastases (*lasB*)
403 and pyocyanin biosynthetic genes. This demonstrates that the bacterial response differs
404 depending on the host environment.

405 In summary, our results show that *P. aeruginosa* regulates several pathways involved
406 in iron starvation, respiration, and virulence mechanisms in a CF ALI model, in response to
407 different environmental cues. Many of these traits have been previously linked to adaptation
408 *in vivo* CF airways (*56*, *57*), thus underscoring the robustness of our infection model.

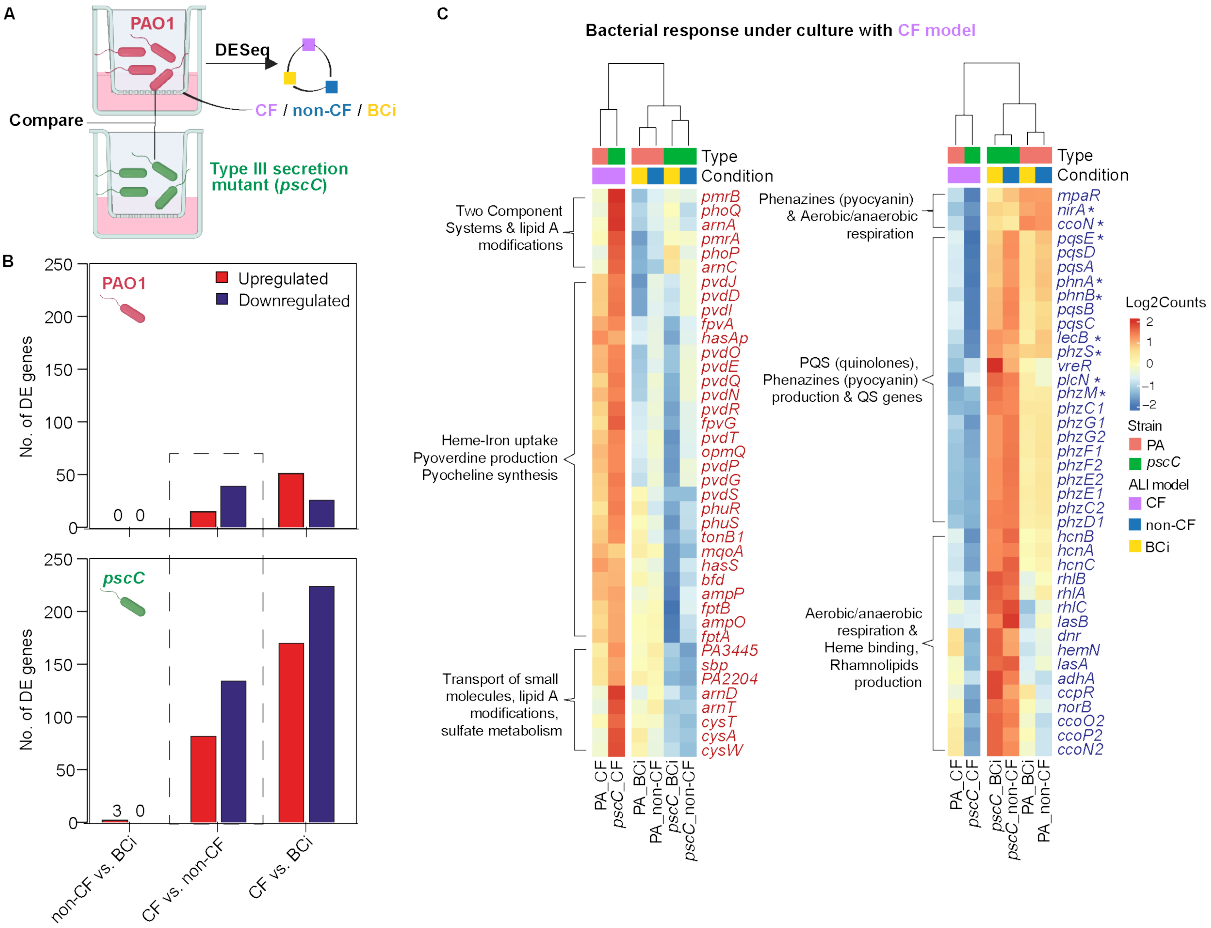

Figure 6. Bacterial response in different ALI models. A) Representation of the differentially expressed gene (DEG) comparison of PAO1 and *pscC* mutant strain transcriptomes analyzed in different ALI models, *i.e.*, non-CF vs. BCi-NS1.1, CF vs. non-CF, and CF. vs BCi-NS1.1. B) Number of DEGs shown as upregulated (red) or downregulated (blue) and separated by strain (PAO1 top and *pscC* mutant strain bottom panel, respectively). An adj p value < 0.05 and $\log_2$ Fold Change ≥ |1.0| was used as cutoff. C) Heatmap of $\log_2$ read counts scaled for each gene (row) selected from categories from Table S6, comparison *pscC* CF vs. non-CF. Each column represents the mean of the three biological replicates sequenced, clustered based on the result of pvclust analysis. Genes with asterisk (*) were differentially expressed in both PAO1 and *pscC* mutant strain, when comparing CF vs. non-CF models. CF: cystic fibrosis; BCi: BCi-NS1.1.

Discussion

425 Persistent bacterial infections are often associated with antibiotic resistance. However, several
426 other mechanisms, such as reduced virulence, slow growth, and immune evasion, have been
427 proposed to explain antibiotic treatment failure (*3*). This underscores the need to understand
428 the infection and colonization processes at the host-pathogen interface beyond antibiotic
429 resistance. Several *in vitro* studies of clinical strains have shown convergence toward low
430 virulent phenotype as chronic infection progresses (*22*, *25*, *40*, *41*). However, molecular
431 changes often poorly reflect *in vivo* conditions due to differing environment and absence of
432 host interactions (*56*, *57*). Recently, specific mutations in *P. aeruginosa* were discovered to be
433 involved in novel adaptive mechanisms that transcend conventional antibiotic resistance,
434 highlighting the need for host-focused approaches to develop more effective strategies for
435 treating bacterial infections (*34*, *38*).

436 To address this, we quantified infection outcomes during the early stages of
437 colonization using different clinical isolates of *P. aeruginosa* by comparing three types of ALI
438 infection models (non-CF, CF, and BCi-NS1.1). We quantified host response including epithelial
439 integrity (TEER), cellular cytotoxicity (LDH), inflammatory response (Interleukin 8), bacterial
440 load (CFU), and localization within the ALI models (confocal microscopy) to provide systematic
441 insight into the infection capabilities of *P. aeruginosa*. Irrespective of the type of ALI model
442 (non-CF, CF, and BCi-NS1.1), colonization was predominantly driven by the intrinsic bacterial
443 virulence potential. Infection clusters were neither based on the genetic background of the
444 strains (*i.e.*, isolates from the same lineage were not always grouped together), nor on the
445 level of adaptation (*i.e.*, late strains did not always show reduced virulence). While high
446 virulence has been identified as a key driver during the early stages of host colonization
447 (clusters 1 and 2), the preferential bacterial localization, either attached to the epithelium
448 (cluster 3) or planktonic (apical) growth (cluster 4), has not previously been shown in clinical
449 isolates. This distinction is highly relevant, since bacterial localization has significant
450 implications for treatment failure (*38*). In our ALI model using CF-derived primary cells, we
451 observed similar infection profiles, regardless of ETI modulator treatment or bacterial strain.
452 This is in agreement with recent works showing that, although there is a reduction of bacterial
453 load in pwCF treated with ETI, bacteria persist in the airway (*10*, *12*). The observed trends
454 provide valuable ground knowledge about the inherent properties of the ALI models
455 employed, as well as about the virulence of the infecting bacteria. Importantly, the ALI model
456 holds predictive potential as it allows evaluation of drug efficacy, immune system activity, host

457 response, and inter-species interactions, which are fundamental to understanding infection
458 progression and improving treatment outcomes.

459 Recent transcriptomics studies have explored *P. aeruginosa* interactions in ALI models
460 (*30*, *32*, *36*, *58*). However, comparative insight into the molecular responses of non-CF, CF,
461 and BCi-NS1.1 ALI models remains limited. To address this gap, we performed dual
462 transcriptomic analysis of *P. aeruginosa* infections across these model systems. Given the
463 biological complexity and technical challenges associated with primary cells, our analysis
464 focused on infections with the reference strain PAO1 and a less virulent *pscC* mutant, since
465 the T3SS plays a key role in early host colonization and invasion (*33*).

466 Importantly, a high correlation between the three types of ALI models was observed
467 and only 2.4 % of the identified genes were differentially expressed across all comparisons.
468 This indicates that the primary response and gene expression profiles are comparable
469 between ALI models independently of the host origin or donor. Similar to earlier research, we
470 found that colonization of host epithelium with *P. aeruginosa* triggers activation of
471 inflammatory pathways, response to bacteria and LPS through upregulation of NF-kβ and
472 TNFα signaling pathways and overexpression of cytokines including IL-6 and IL-17 signaling
473 (*30*, *36*). In agreement with the latter, infections carried out with eight different donors (n = 3,
474 non-CF and n = 5, CF) showed similar trends in IL-8 secretion for PAO1 across the different ALI
475 models. On the other hand, deletion of the *pscC* gene induced fewer host DEGs related to
476 inflammation compared to PAO1. This aligns well with infection readouts, where the *pscC*
477 mutant strain exhibited intermediate virulence between PAO1 and the more adapted clinical
478 strains.

479 Upon infection and depending on the availability of nutrients and/or host signals, *P.*
480 *aeruginosa* tightly controls the regulation of a wide array of virulence factors involved in host-
481 mediated respiratory infections (*59*). In our CF ALI model, both PAO1 and *pscC* mutant strain
482 limited the expression of *lasB*, a principal extracellular virulence factor, and the biosynthesis
483 of pyocyanin, both contributing to inflammation and epithelial disruption (*60*). The
484 downregulation of these genes may enable the bacteria to evade the immune system and
485 reduce host inflammation, as observed in our infected CF ALI models, which showed fewer
486 DEGs (n = 442) compared to non-CF (n = 761) and BCi-NS1.1 ALI models (n = 804) models.
487 Strikingly, the interaction between CF ALI models and the *pscC* mutant strain showed a more
488 complex regulation resembling many of the features already seen in clinical CF isolates.

489 Besides phenazine biosynthesis, the *pscC* mutant strain also showed downregulation of the
490 PQS system and rhamnolipid production, mirroring key features of CF late chronic strains (*56*).
491 Another example is the high expression of genes involved in the production and
492 transportation of siderophores pyoverdine (*pvd*) and pyochelin (*pch*), as well as the
493 assimilation of heme (*phu* and *has* systems) (*57*), suggesting limited accessibility of these
494 micronutrients in CF ALI models relative to non-CF.

495 While infection models allow for a more representative analysis of bacterial
496 phenotypes, they also have some limitations. It was, indeed, surprising that only a few isolates
497 showed significant differences in one or two infection outcomes between non-CF and CF ALI
498 models. This result may be influenced by several factors: a) the ALI model does not fully
499 replicate the *in vivo* lung environment, which is influenced by the presence of immune cells,
500 potential antibiotic exposure, and oxygen and micronutrient gradients, b) the chosen infection
501 time points (14 or 38 h) may be sub-optimal for detecting subtle host response patterns, c)
502 the enclosed nature of the ALI transwells may limit mucociliary clearance, or d) the absence
503 of a residing airway microbiota, which could modulate host-pathogen interactions. Therefore,
504 further investigations are required to systematically evaluate the contribution of each of these
505 parameters.

506 Altogether, we explored the virulence potential of clinically persistent clones of *P.*
507 *aeruginosa* when colonizing different airway epithelial tissues grown at the ALI interface. We
508 covered a variety of bacterial lineages and host donors and defined clusters of infection
509 properties. Furthermore, we quantified the global transcriptional response of both host and
510 pathogen upon infection. Our data foster the need for studies using host-pathogen models to
511 recapitulate the *in vivo* conditions of pathogenic diseases. Moreover, given the more
512 appropriate physiological environment, ALI models serve as a platform for evaluating
513 treatment efficacy and identifying novel therapies for the treatment of persistent infections.
514 Yet, further studies implementing immune cells, antibiotic treatment, and other infecting
515 species are needed to understand infection progression, antibiotic treatment failure, and new
516 mechanisms of persistence.
517
518

519 **Materials and Methods**

520 **Ethical approval and consent to participate**

521 This study was approved by the local ethics committee of the Capital Region of Denmark
522 (Region Hovedstaden), registration number H-20024750. All patients provided informed
523 consent to participate in the study and for the publication of associated results and pertinent
524 clinical data. Pseudonymization of patient information was performed to untie any links that
525 could lead to patient identification.

526

527 **Primary basal cell extraction, cell lines and culture.**

528 Primary basal cells were obtained from nasal brushes, nasal polyps, and distal lung biopsies
529 from pwCF (n = 10) and non-CF (n = 5) donors. Details on sample source and CFTR mutation
530 are provided in Table S2 separated according to assay.

531 Nasal brushes were obtained with a 2.5 mm cytology brush and nasal polyps, and lung
532 biopsies were surgically removed. All samples were placed in fresh culture media,
533 supplemented with primocin (Invivogen, ant-pm-05), gentamicin/amphotericin solution
534 (Gibco, Cat #10184583) and pen/strep (Gibco, Cat #15140122), immediately following
535 collection. Nasal brush samples were homogenized by resuspension, whereas nasal polyps
536 and lung biopsies were disrupted by scraping and dissection to release basal cells. To remove
537 any blood and mucus, nasal polyps and lung biopsies were washed three times in fresh media.
538 Next, samples were centrifuged at 300 x g for 5 min at room temperature (R/T) and cell pellets
539 were resuspended in PneumaCult™-Ex Plus Medium, with PneumaCult™-Ex Plus 50X
540 (STEMCELL Technologies, Cat #05040), according to manufacturer's instructions,
541 supplemented with 96 ng/mL hydrocortisone (STEMCELL Technologies, Cat #07925) and 10
542 µM ROCK inhibitor (Y-27632) (Tocris Bioscience Cat #1254), hereafter ExPlus media. BCi-NS1.1,
543 Basal Cells Immortalized-NonSmoker 1.1, an hTERT expressing airway cell line, and primary
544 cells (non-CF and CF), were seeded into culture flasks (Greiner, item no. 690160 & item no.
545 658175) and maintained in ExPlus media. When reaching 80 % confluence, cells were
546 passaged by detachment with TrypLE (Gibco Cat #12563011) for further expansion or for
547 seeding into transwells for ALI culture. Specifically for primary cells (non-CF and CF), cell
548 culture flasks were pre-coated with human type-I collagen (Gibco, Cat #A1048301), ExPlus
549 media was further supplemented with antibiotics as described above, and only passage 1-3

550 were used for ALI models. All cells were maintained at standard conditions, 37 °C, 5 % CO2 in
551 a humidified incubator.
552
553 **Air-liquid interface (ALI)**
554 To establish ALI models, 1.5 x 10^5 basal cells from non-CF, CF, and BCi-NS1.1 were seeded in
555 transwells (6.5 cm^2, 0.4 µm pores) (Corning Life Sciences product no. 3470) pre-coated with
556 human type-I collagen (Gibco, Cat #A1048301). ALI models were cultured in ExPlus media,
557 prepared as described, added to the apical and basolateral compartment. Upon full
558 confluence, ALI was established by aspirating the media from both compartments, and adding
559 PneumaCult™-ALI Medium, with PneumaCult™-ALI 10X Supplement and PneumaCult™-ALI
560 Maintenance Supplement (100X), according to manufacturer's instructions (STEMCELL
561 Technologies, Cat #05001), supplemented with 480 ng/mL hydrocortisone (STEMCELL
562 Technologies, Cat #07925) and 4 µg/mL heparin (STEMCELL Technologies, Cat #07980) to the
563 basolateral compartment. ALI models were cultured for a minimum of 28 days, media was
564 refreshed as required. When necessary, ALI models were rinsed apically with PBS to remove
565 excess mucus. ALI models were maintained at standard conditions, 37 °C, 5 % CO2 in a
566 humidified incubator.
567
568 **ETI modulator treatment of infected and noninfected ALI models**
569 On day 28 of ALI culturing, a combined CFTR-modulator treatment of 3 µM elexacaftor (VX-
570 445, MedChemExpress), 10 µM tezacaftor (VX-661, Selleck Chemicals LLC), and 5 µM ivacaftor
571 (VX-770, Selleck Chemicals LLC), hereafter ETI, was added for 24 h to the basolateral medium.
572 ETI compounds were prepared fresh before each experiment. Untreated controls were treated
573 with an equal volume of DSMO. For infection studies, ALI models were treated ± ETI for 24 h
574 prior to infection, as described above. Infections were carried out with PAO1 (14 h), DK01_I
575 (14 h), and DK02_L (38 h), adding fresh ETI at the start of infection.
576
577 **Transepithelial electrical conductance (TEEC) measurement**
578 TEEC is calculated from the reciprocal value of TEER measurements:
579
580 $$Transepithelial\ electrical\ conductance(TEEC) = \frac{1}{Resistance} = \frac{1}{TEER}$$

581 $$\Delta TEEC = TEEC(\max) - TEEC(inhib)$$

582

583 TEER was measured after maximal CFTR stimulation with forskolin (TargetMol, Cat #T2939)
584 and genistein (TargetMol, Cat #T1737), and subsequent inhibition with PPQ-102 (TargetMol,
585 Cat #T1874), before converted to TEEC. First, Coon's modified Ham's F12 medium without
586 $NaHCO_3$ (DiagnoCine, Cat #AT146), supplemented 20 mM Na-Hepes (SigmaAldrich) (pH 7.3),
587 was added to the apical and the basolateral compartment, and equilibrated for 1 h, after
588 which, a baseline TEER was measured. Following, 10 µM amiloride (SigmaAldrich, Cat #A7410)
589 was added to the apical compartment. Next, apical and basolateral medium was refreshed,
590 and 10 µM forskolin and 50 µM genistein was added. Subsequently, a solution containing 30
591 µM PPQ-102 (CFTR inhibitor) was added to the apical compartment. Between each step, a 10
592 min incubation time was allowed, after which TEER was measured, and subsequently
593 converted to TEEC. ALI models, non-CF and CF, were tested in at least three technical
594 replicates.

595

596 **Clinical strains, growth conditions and fluorescent tagging**

597 Strains used in this study are summarized in Table S1. Clinical strains were obtained from
598 sputum samples from pwCF attending or who have attended the Copenhagen Cystic Fibrosis
599 Center at University Hospital Rigshospitalet, Copenhagen, Denmark. Sputum sampling is part
600 of the routine visits to the CF clinic and was not performed for the purpose of this research.
601 All clinical strains except DK01_E and DK02_E, were previously sequenced and their genomic
602 and transcriptomic profiles characterized (*40*).

603 *P. aeruginosa* reference strains PAO1, PA14, and C-clone were obtained from the Leibniz
604 Institute DSMZ collection with references DSM22644, DSM19882, and DSM29238,
605 respectively. Additionally, an isogenic *pscC* mutant strain (PAO1 background), previously
606 constructed and used for infection studies in our lab was included (*17*).

607 All strains were tagged with a superior green fluorescent protein (sfGFP) to enable
608 visualization by confocal microscopy. Bacterial strains were GFP-tagged by 4 parental mating
609 using the miniTn7 delivery plasmid with rhaSR-PrhaBAD inducible promoter (pJM220) (*61*).
610 The plasmid was engineered to accommodate the sfGFP gene. Transformants were selected
611 on *Pseudomonas* isolation agar supplemented with 30 µg/mL gentamicin (SigmaAldrich, Cat

612 #G3632). The final sfGFP-tagged strains were verified by fluorescence using a Leica DM4000
613 B epifluorescence microscope and growth rate (Fig S8).
614
615 **Phenotypic characterization of *P. aeruginosa* strains**
616 GFP-tagged strains were characterized based on their growth in synthetic cystic fibrosis media
617 (SCFM), prepared as previously described(*62*), bacterial movement, and antibiotic
618 susceptibility profiles. Briefly, single colonies were picked and grown on liquid Luria-Bertani
619 broth (LB) cultures. Cultures were standardized to OD_{600} = 0.1 and further diluted to OD_{600} =
620 0.01 in SCFM media and growth was recorded every 15 min for 18 h in a 96 well plate reader
621 at 37 °C with continuous shaking. Doubling times and growth rate estimations were calculated
622 using Graph Pad Prism software (v 10.2.2), focusing on the exponential part of the growth
623 curve. For swimming assay, 2 µL of the OD_{600} = 0.1 cultures were plated on the center of
624 tryptone broth plates (10 g/L tryptone, 5 g/L NaCl) with 0.25 % agarose. Motility diameter was
625 measured after incubation for 6 h at 37 °C and additional 16 h, at R/T. For antimicrobial
626 susceptibility, the microdilution method from EUCAST was used (The European Committee on
627 Antimicrobial Susceptibility Testing 2023). Cultures were standardized to Mc Farland (5 x 10^5
628 CFU/mL) and grown in Müller-Hinton broth with serial fold dilutions of either tobramycin
629 (SigmaAldrich, Cat #T4014), ceftazidime (SigmaAldrich, Cat #C3809), or ciprofloxacin
630 (SigmaAldrich, Cat #17850) for 16 h in 96 well plates at 37 °C with continuous shaking. MIC
631 was calculated as the concentration of antimicrobial required for complete growth inhibition
632 of the strain as detected by the naked eye. All phenotypic experiments were performed with
633 three independent cultures.
634
635 **Infection of ALI models with *P. aeruginosa***
636 Overnight *P. aeruginosa* cultures were standardized to OD_{600} = 0.05 (reference, early, and
637 intermediate strains) or OD_{600} = 0.1 (late strains) and grown until mid-exponential phase in
638 5 mL of LB medium. Subsequently, 1 mL of culture was centrifuged at 5000 × g for 5 min, and
639 bacterial pellets were washed and resuspended in PBS at a concentration of 1 x 10^7 CFU/mL.
640 For each strain, the OD:CFU ratio was tested in triplicates to achieve reproducible results. A
641 final of 1 x 10^3 CFU was used to inoculate the apical side of ALI models. Mock infected samples
642 were inoculated with an equal volume PBS. Infected ALI models were incubated at 37 °C, 5 %
643 CO_2 in a humidified incubator for the specified duration required to characterize the infection

644 (14 h for reference, early, and intermediate strains, and 38 h for late strains). At the end of
645 infection, 200 µL of PBS was added apically, and TEER was measured.
646 Subsequently, apical PBS and basolateral media was collected for CFU quantification by plating
647 10 µL of serial dilutions on LB-agar plates. Remaining sample was preserved at −80 °C for
648 downstream analysis of LDH and IL-8. For quantification of attached bacteria, 200 µL of Triton
649 X-100 (0.1 % in PBS), with no harm to bacteria (*34*), was added apically, the epithelium
650 disrupted using a cell scraper, and CFU were quantified as described above.
651
652 **Transepithelial electrical resistance (TEER)**
653 Transepithelial electrical resistance (TEER) was measured prior to and immediately at the end
654 of infection using the EVOM2 (World Precision Instruments) and the STX2 electrode (World
655 Precision Instruments). The electrode was submerged into 200 µL PBS at the apical
656 compartment and 400 µL media in the basolateral compartment.
657
658 **Immunofluorescence staining and confocal microscopy**
659 ALI models were fixed in 4 % paraformaldehyde for 20 min, at 4 °C. Following, ALI models were
660 washed 3 times with PBS, and incubated in blocking buffer (0.1 % Triton X-100, 1 % saponin,
661 3 % BSA in PBS) for 1 h, at R/T. Next, ALI models were incubated with primary antibodies
662 diluted in staining solution containing 3 % BSA and 1 % saponin in PBS at 4 °C, overnight. Next
663 day, ALI models were washed 3 times in PBS and incubated with secondary antibodies and
664 dyes, diluted in staining solution, for 2 h, at R/T. After staining, membranes were excised from
665 the transwells and mounted onto microscope slides with VECTASHIELD® Antifade Mounting
666 Medium (VWR, Cat #VECTH-1000). Images were acquired with the Leica Stellaris 8 Confocal
667 Microscope (40X, Oil objective) and analyzed using the LasX software 1.4.4.26810 (Leica) and
668 Imaris 10.1.0 software.
669
670 **Antibodies and dyes**
671 The following antibodies and dyes were used: anti-MUC5AC (Invitrogen Cat #MA5-12178,
672 1:100), anti-CFTR 570 (kind gift from cystic fibrosis foundation, 1:100), Phalloidin-Alexa Fluor
673 555 (Invitrogen Cat #A30106, 1:400). Alexa Fluor-647 Goat anti-mouse (Invitrogen Cat
674 #A21235, 1:500) and DAPI nuclear dye (Thermo Scientific Cat #62248, 1:750).
675

676 **Lactate dehydrogenase (LDH) assay**

677 LDH release was determined with the CyQUANT™ LDH Cytotoxicity Assay Kit (Invitrogen, Cat
678 #C20301) according to manufacturer's instructions. For this, 50 µL of basolateral media was
679 taken from ALI models, and absorbance was measured at 680 nm and 490 nm. All samples
680 were analyzed in triplicates.

681

682 **Interleukin-8 (IL-8) quantification**

683 IL-8 secretion was measured with the Human IL-8/CXCL8 DuoSet ELISA kit (Bio-Techne, Cat
684 #DY208) according to manufacturer's instructions. Basolateral media was diluted 1:10 and
685 absorbance was measured at 450 nm and 540 nm. All samples were analyzed in triplicates.

686

687 **RNA extraction from ALI cultures and sequencing library preparation**

688 Basal cells derived from a lung biopsy of a non-CF donor (non-CF 16), a nasal brush from one
689 pwCF (CF14), and the BCi-NS1.1 cell line were used to generate ALI models. These models
690 were infected with either PAO1, *pscC* mutant strain, or mock infected in six independent
691 transwells. ALI models and infections followed the same procedures as described for other
692 samples in this study. Infection outcomes were consistent with the experimental variability
693 observed across donors (Table S2).

694 Total RNA was extracted using the Qiagen RNeasy Plus Mini kit, following the manufacturer´s
695 protocol. Briefly, after infection and TEER measurements, PBS was removed from the apical
696 compartment, and 300 µL of RNA protect Cell Reagent was added. Adherent cells were
697 detached by pipetting without the need of enzymatic dissociation and two transwells from
698 the same condition were pooled per 300 µL of sample and frozen at -80 until RNA extraction.
699 For enzymatic lysis, samples were thawed, centrifuged to remove RNA protect, then
700 resuspended in 1 mL of RNA-se free water containing 1 mg/mL of lysozyme, and incubated for
701 30 min at 37°C. Samples were then centrifuged and resuspended in 600 µL RLT Buffer (with β-
702 mercaptoethanol), and RNA was extracted following the Qiagen protocol to recover fragments
703 >200 nt. RNA was quantified using the Qubit® RNA BR Assay kit (Invitrogen), and integrity
704 assessed with an Agilent 2100 Bioanalyzer using the RNA Nano kit. All samples had DV_{200}
705 values (percentage of RNA fragments >200 nt) ranging from 50 % to 75 % and were included
706 in downstream processing.

707 2 µg of eluted RNA were treated with DNAse I (Invitrogen) for 30 min at 37°C in a final volume
708 of 50 µL. The treated RNA was purified using Qiagen columns by combining 150 µL RLT Buffer
709 (without β-mercaptoethanol), 150 µL 95-100 % ethanol, and 50 µL RNA sample. Following two
710 washes with RPE buffer, RNA was eluted in 20-25 µL RNA-se free water.
711 A total of 500 ng of RNA per sample was used to prepare sequencing libraries using the
712 Illumina Stranded Total RNA Prep with Ribo-Zero Plus kit. Sequencing was performed on an
713 Illumina NextSeq 500 system using a high output kit, generating a minimum of 30 million (M)
714 single end 75 bp reads per sample.
715 As bacterial transcripts represent only a small fraction of the total RNA within host cells (*63*),
716 RNA was extracted from two independent infected transwells and combined to form a single
717 biological replicate. Each condition included three such replicates, and no more than 12
718 samples were pooled for sequencing run. This approach enhanced the recovery of bacterial
719 RNA, yielding between 2.5 M to 10 M reads per sample depending on the bacterial strain and
720 cell type (Fig S9, Table S7). For samples infected with the *pscC* mutant strain (non-CF-*pscC* 1-
721 3, CF-*pscC* 2-3, BCi-*pscC* 1-3), a second sequencing round was performed to achieve a
722 minimum threshold of 1 M reads mapping to the *Pseudomonas* genome. Table S7 lists the
723 sequencing yields for both runs (BCi-*pscC* 1a and BCi-*pscC* 1b, etc.).
724
725 **Host-pathogen transcriptome analysis**
726 Sequencing reads were analyzed with our in-house pipeline updated for host-pathogen
727 samples (*64*). Briefly, low-quality bases and contaminant adapters were trimmed using
728 Trimmomatic (v 0.35), discarding reads shorter than 35 nt. Reads were further processed using
729 the SortMeRNA tool (v 2.1) to remove reads generated from residual rRNA transcripts. High-
730 quality human and bacterial reads were separated *in silico* by mapping reads using the BWA
731 aligner and MEM algorithm against the human genome assembly GRCh38.p9 retrieved from
732 the NCBI database. Reads not mapping on the human genome were used as input for
733 analyzing the transcriptionally active *P. aeruginosa* population mapping against *P. aeruginosa*
734 PAO1 genome (NCBI: NC_002516.2) using BWA (0.7.15-r1140) aligner and MEM algorithm
735 with default parameters.
736
737 **Gene expression analysis**

Mapped reads from both host and *P. aeruginosa* were quantified using htseq-count (v 0.7.2). Resulting count tables were imported into R for differential gene expression (DEG) analysis. For host data, genes with ≥10 reads in at least three samples were retained, resulting in a filtered dataset of 18746 genes. Counts were normalized across all samples using the variance stabilizing transformation (VST-normalization) in the DESEq2 package (v 1.44.0) with the option blind = TRUE (*65*). For bacterial reads, only genes with ≥10 reads in all replicate samples were retained, yielding 4255 *P. aeruginosa* genes. VST-normalized counts were used for exploratory analysis including principal component analysis (PCA) using `plotPCA()` function, visualized with `ggplot()`, and hierarchical clustering analysis (HCA). When necessary, correlation plots were generated from normalized count data using Pearson's correlation coefficients, with significance values reported. Heatmaps of selected gene sets were generated using `pheatmap()`, based on condition-wise replicate means.

DEGs were identified from DESeq2 results using the `results()` function with the `contrast` argument for pairwise comparisons. Genes were considered differentially expressed with a $\log_2$ Fold Change ≥ |1.0| and an adjusted p value ≤ 0.05.

Significant host DEGs were analyzed for gene set enrichment analyses with the "Human Hallmark" collection from the Molecular Signature Database (MsigDB). Gene sets were retrieved with `msigdbr()`, and enrichment was performed using the `GSEA()` with the following parameters: `minGSSize=5`, `maxGSSize=500`, `pvalueCutoff=0.05`, `pAdjustMethod="BH"`. Additional enrichment analysis using the KEGG database was performed using `gseKEGG()` under the same parameters. When overlapping pathways were identified (e.g., "response to lipid" vs. "cellular response to lipid"), the term with the lowest adjusted p value was selected.

For bacterial DEGs, functional enrichment was conducted using $\log_2$ Fold Change values and gene-term associations from COGs and KEGG annotations based on *P. aeruginosa* PAO1 data from Pseudomonas.com, via `GSEA()` and `gseKEGG()` with `organism="pae"`.

To assess overlap among DEG lists, UpSet plots were generated using the `UpSet()` function in R.

Data sharing

768 Raw sequence data supporting the results of this work are available as SRA BioProject under
769 Accession No. PRJNA1153754 and accession numbers from individual BioSamples and
770 sequences is summarized in Table S7. All data is available in the publication.
771
772 **Author Contribution Statement**
773 **Claudia Antonella Colque:** Methodology, Formal analysis, Investigation, Data curation,
774 Visualization, Writing – original draft, Writing – review & editing. **Signe Lolle:** Methodology,
775 Formal analysis, Investigation, Writing – review & editing. **Ruggero La Rosa:** Formal analysis,
776 Data curation, Visualization, Writing – original draft, Writing – review & editing. **Maria Pals**
777 **Bendixen:** Investigation, Writing – review & editing. **Asha M. Rudjord-Levann:** Formal
778 analysis, Writing – review and editing. **Filipa Bica Simões:** Methodology, Formal analysis,
779 Investigation, Writing – original draft, Writing – review & editing. **Kasper Aanæs**: Resources.
780 **Søren Molin:** Conceptualization, Supervision, Writing – review & editing. **Helle Krogh**
781 **Johansen:** Conceptualization, Funding acquisition, Resources, Supervision, Writing – review &
782 editing.
783
784 **Acknowledgments**
785 The authors thank the Danish pwCF and the non-CF donors who participated in this study,
786 Laura Elisabeth Bojesen Haapalo and Rene Horsleben Petersen (Department of Cardiothoracic
787 Surgery, Copenhagen University Hospital, Rigshospitalet, Denmark) for providing and assisting
788 with lung tissue samples, and the nurses from Rigshospitalet CF clinic assisting with patient
789 recruitment and sample collection. We thank the cystic fibrosis foundation (CFF) for providing
790 the CFTR anti570 antibody, and Ronald G. Cristal (Weil Cornell Medical College, New York,
791 USA) for providing the BCi-NS1.1 cell line. This research was funded by a Challenge Grant (Ref.
792 nr.: NNF19OC0056411) and a grant from The John and Birthe Meyer Foundation awarded to
793 HKJ. HKJ and SM were supported by a grant from CAG - Greater Copenhagen Health Science
794 Partners (GCHSP), 2020. The work at the Novo Nordisk Foundation Center for Biosustainability
795 (CfB) is supported by the Novo Nordisk Foundation (Ref. nr.: NNF10CC1016517). We thank the
796 Infection Microbiology group (Oihane Irazoqui Sanchez, Pablo Laborda Martínez, Janus Anders
797 Juul Haagensen) for their insightful comments and discussions. We thank Elio Rossi
798 (Department of Biosciences, University of Milan, Italy) for his advice on transcriptomics

799 analysis, and Nicoletta Pedemonte (IRCCS Institute Gaslini, Genova, Italy) for her assistance in
800 modulator treatment assays.
801

References

1. R. La Rosa, H. K. Johansen, S. Molin, Persistent Bacterial Infections, Antibiotic Treatment Failure, and Microbial Adaptive Evolution. *Antibiotics* **11**, 419 (2022).

2. E. F. Haney, R. E. W. Hancock, Addressing Antibiotic Failure—Beyond Genetically Encoded Antimicrobial Resistance. *Front. Drug. Discov.* **2**, 892975 (2022).

3. R. La Rosa, S. Molin, H. K. Johansen, Pseudomonas aeruginosa: persistence beyond antibiotic resistance. *Trends in Microbiology*, S0966842X25001519 (2025).

4. D. N. Sheppard, M. J. Welsh, Structure and Function of the CFTR Chloride Channel. *Physiological Reviews* **79**, S23–S45 (1999).

5. B. P. O'Sullivan, S. D. Freedman, Cystic fibrosis. *The Lancet* **373**, 1891–1904 (2009).

6. T. A. Douglas, S. Brennan, S. Gard, L. Berry, C. Gangell, S. M. Stick, B. S. Clements, P. D. Sly, Acquisition and eradication of P. aeruginosa in young children with cystic fibrosis. *European Respiratory Journal* **33**, 305–311 (2008).

7. M. Rosenfeld, J. Emerson, F. Accurso, D. Armstrong, R. Castile, K. Grimwood, P. Hiatt, K. McCoy, S. McNamara, B. Ramsey, J. Wagener, Diagnostic accuracy of oropharyngeal cultures in infants and young children with cystic fibrosis. *Pediatr. Pulmonol.* **28**, 321–328 (1999).

8. H. G. M. Heijerman, E. F. McKone, D. G. Downey, E. Van Braeckel, S. M. Rowe, E. Tullis, M. A. Mall, J. J. Welter, B. W. Ramsey, C. M. McKee, G. Marigowda, S. M. Moskowitz, D. Waltz, P. R. Sosnay, C. Simard, N. Ahluwalia, F. Xuan, Y. Zhang, J. L. Taylor-Cousar, K. S. McCoy, K. McCoy, S. Donaldson, S. Walker, J. Chmiel, R. Rubenstein, D. K. Froh, I. Neuringer, M. Jain, K. Moffett, J. L. Taylor-Cousar, B. Barnett, G. Mueller, P. Flume, F. Livingston, N. Mehdi, C. Teneback, J. Welter, R. Jain, D. Kissner, K. Patel, F. J. Calimano, J. Johannes, C. Daines, T. Keens, H. Scher, S. Chittivelu, S. Reddivalam, R. C. Klingsberg, L. G. Johnson, S. Verhulst, P. Macedo, D. Downey, G. Connett, E. Nash, N. Withers, T. Lee, M. Bakker, H. Heijerman, F. Vermeulen, E. Van Braeckel, C. Knoop, E. De Wachter, R. Van Der Meer, P. Merkus, C. Majoor, Efficacy and safety of the elexacaftor plus tezacaftor plus ivacaftor combination regimen in people with cystic fibrosis homozygous for the F508del mutation: a double-blind, randomised, phase 3 trial. *The Lancet* **394**, 1940–1948 (2019).

9. M. M. Szabo, S. E. Foushee, C. M. McPheeters, A. R. O'Hagan, A. M. Ramirez, E. A. O'Reilly, Impact of elexacaftor/tezacaftor/ivacaftor on respiratory colonization in an adult cystic fibrosis clinic. *The American Journal of the Medical Sciences* **367**, 337–342 (2024).

10. C. R. Armbruster, Y. K. Hilliam, A. C. Zemke, S. Atteih, C. W. Marshall, J. Moore, J. Koirala, L. Krainz, J. R. Gaston, S. E. Lee, V. S. Cooper, J. M. Bomberger, Persistence

and evolution of *Pseudomonas aeruginosa* following initiation of highly effective modulator therapy in cystic fibrosis. *mBio* **15**, e00519-24 (2024).

11. E. L. Ledger, D. J. Smith, J. J. Teh, M. E. Wood, P. E. Whibley, M. Morrison, J. B. Goldberg, D. W. Reid, T. J. Wells, Impact of CFTR Modulation on *Pseudomonas aeruginosa* Infection in People With Cystic Fibrosis. *The Journal of Infectious Diseases* **230**, e536–e547 (2024).

12. D. P. Nichols, S. J. Morgan, M. Skalland, A. T. Vo, J. M. Van Dalfsen, S. B. P. Singh, W. Ni, L. R. Hoffman, K. McGeer, S. L. Heltshe, J. P. Clancy, S. M. Rowe, P. Jorth, P. K. Singh, Pharmacologic improvement of CFTR function rapidly decreases sputum pathogen density, but lung infections generally persist. *Journal of Clinical Investigation* **133**, e167957 (2023).

13. J. A. Bartell, L. M. Sommer, R. L. Marvig, M. Skov, T. Pressler, S. Molin, H. K. Johansen, Omics-based tracking of *Pseudomonas aeruginosa* persistence in “eradicated” cystic fibrosis patients. *Eur Respir J* **57**, 2000512 (2021).

14. J. Mésinèle, M. Ruffin, A. Kemgang, L. Guillot, P.-Y. Boëlle, H. Corvol, Risk factors for Pseudomonas aeruginosa airway infection and lung function decline in children with cystic fibrosis. *Journal of Cystic Fibrosis* **21**, 45–51 (2022).

15. S. L. Gellatly, R. E. W. Hancock, *Pseudomonas aeruginosa* : new insights into pathogenesis and host defenses. *Pathogens Disease* **67**, 159–173 (2013).

16. R. La Rosa, H. K. Johansen, S. Molin, Adapting to the Airways: Metabolic Requirements of Pseudomonas aeruginosa during the Infection of Cystic Fibrosis Patients. *Metabolites* **9**, 234 (2019).

17. B. H. Pedersen, F. B. Simões, I. Pogrebnyakov, M. Welch, H. K. Johansen, S. Molin, R. La Rosa, Metabolic specialization drives reduced pathogenicity in Pseudomonas aeruginosa isolates from cystic fibrosis patients. *PLoS Biol* **22**, e3002781 (2024).

18. E. Rossi, R. La Rosa, J. A. Bartell, R. L. Marvig, J. A. J. Haagensen, L. M. Sommer, S. Molin, H. K. Johansen, Pseudomonas aeruginosa adaptation and evolution in patients with cystic fibrosis. *Nat Rev Microbiol* **19**, 331–342 (2021).

19. N. Cramer, J. Klockgether, K. Wrasman, M. Schmidt, C. F. Davenport, B. Tümmler, Microevolution of the major common *Pseudomonas aeruginosa* clones C and PA14 in cystic fibrosis lungs. *Environmental Microbiology* **13**, 1690–1704 (2011).

20. S. Fischer, S. Dethlefsen, J. Klockgether, B. Tümmler, Phenotypic and Genomic Comparison of the Two Most Common ExoU-Positive Pseudomonas aeruginosa Clones, PA14 and ST235. *mSystems* **5**, e01007-20 (2020).

21. L. Jelsbak, H. K. Johansen, A.-L. Frost, R. Thøgersen, L. E. Thomsen, O. Ciofu, L. Yang, J. A. J. Haagensen, N. Høiby, S. Molin, Molecular Epidemiology and Dynamics of *Pseudomonas aeruginosa* Populations in Lungs of Cystic Fibrosis Patients. *Infect Immun* **75**, 2214–2224 (2007).

22. T. Markussen, R. L. Marvig, M. Gómez-Lozano, K. Aanæs, A. E. Burleigh, N. Høiby, H. K. Johansen, S. Molin, L. Jelsbak, Environmental Heterogeneity Drives Within-Host Diversification and Evolution of Pseudomonas aeruginosa. *mBio* **5**, e01592-14 (2014).

23. U. Romling, A. Kader, D. D. Sriramulu, R. Simm, G. Kronvall, Worldwide distribution of Pseudomonas aeruginosa clone C strains in the aquatic environment and cystic fibrosis patients. *Environ Microbiol* **7**, 1029–1038 (2005).

24. A. Weimann, A. M. Dinan, C. Ruis, A. Bernut, S. Pont, K. Brown, J. Ryan, L. Santos, L. Ellison, E. Ukor, A. P. Pandurangan, S. Krokowski, T. L. Blundell, M. Welch, B. Blane, K. Judge, R. Bousfield, N. Brown, J. M. Bryant, I. Kukavica-Ibrulj, G. Rampioni, L. Leoni, P. T. Harrison, S. J. Peacock, N. R. Thomson, J. Gauthier, J. L. Fothergill, R. C. Levesque, J. Parkhill, R. A. Floto, Evolution and host-specific adaptation of *Pseudomonas aeruginosa*. *Science* **385**, eadi0908 (2024).

25. L. Yang, L. Jelsbak, R. L. Marvig, S. Damkiær, C. T. Workman, M. H. Rau, S. K. Hansen, A. Folkesson, H. K. Johansen, O. Ciofu, N. Høiby, M. O. A. Sommer, S. Molin, Evolutionary dynamics of bacteria in a human host environment. *Proc. Natl. Acad. Sci. U.S.A.* **108**, 7481–7486 (2011).

26. T. Bjarnsholt, M. Whiteley, K. P. Rumbaugh, P. S. Stewart, P. Ø. Jensen, N. Frimodt-Møller, The importance of understanding the infectious microenvironment. *The Lancet Infectious Diseases* **22**, e88–e92 (2022).

27. L. Mahieu, L. Van Moll, L. De Vooght, P. Delputte, P. Cos, *In vitro* modelling of bacterial pneumonia: a comparative analysis of widely applied complex cell culture models. *FEMS Microbiology Reviews* **48**, fuae007 (2024).

28. Z. Prytherch, C. Job, H. Marshall, V. Oreffo, M. Foster, K. BéruBé, Tissue-Specific Stem Cell Differentiation in an in vitro Airway Model. *Macromolecular Bioscience* **11**, 1467–1477 (2011).

29. S. Silva, J. Bicker, A. Falcão, A. Fortuna, Air-liquid interface (ALI) impact on different respiratory cell cultures. *European Journal of Pharmaceutics and Biopharmaceutics* **184**, 62–82 (2023).

30. M. Tang, S. Liao, J. Qu, Y. Liu, S. Han, Z. Cai, Y. Fan, L. Yang, S. Li, L. Li, Evaluating Bacterial Pathogenesis Using a Model of Human Airway Organoids Infected with Pseudomonas aeruginosa Biofilms. *Microbiol Spectr* **10**, e02408-22 (2022).

31. R. A. Prescott, A. P. Pankow, M. De Vries, K. M. Crosse, R. S. Patel, M. Alu, C. Loomis, V. Torres, S. Koralov, E. Ivanova, M. Dittmann, B. R. Rosenberg, A comparative study of in vitro air–liquid interface culture models of the human airway epithelium evaluating cellular heterogeneity and gene expression at single cell resolution. *Respir Res* **24**, 213 (2023).

32. G. R. Lewin, A. Kapur, D. M. Cornforth, R. P. Duncan, F. L. Diggle, D. A. Moustafa, S. A. Harrison, E. P. Skaar, W. J. Chazin, J. B. Goldberg, J. M. Bomberger, M. Whiteley,

Application of a quantitative framework to improve the accuracy of a bacterial infection model. *Proc. Natl. Acad. Sci. U.S.A.* **120**, e2221542120 (2023).

33. A. L. Swart, B.-J. Laventie, R. Sütterlin, T. Junne, L. Lauer, P. Manfredi, S. Jakonia, X. Yu, E. Karagkiozi, R. Okujava, U. Jenal, Pseudomonas aeruginosa breaches respiratory epithelia through goblet cell invasion in a microtissue model. *Nat Microbiol* **9**, 1725–1737 (2024).

34. L. Goltermann, P. Laborda, O. Irazoqui, I. Pogrebnyakov, M. P. Bendixen, S. Molin, H. K. Johansen, R. La Rosa, Macrolide resistance through uL4 and uL22 ribosomal mutations in Pseudomonas aeruginosa. *Nat Commun* **15**, 8906 (2024).

35. L. A. Meirelles, E. Vayena, A. Debache, E. Schmidt, T. Rossy, T. Distler, V. Hatzimanikatis, A. Persat, Pseudomonas aeruginosa faces a fitness trade-off between mucosal colonization and antibiotic tolerance during airway infection. *Nat Microbiol* **9**, 3284–3303 (2024).

36. C. Pleguezuelos-Manzano, W. A. G. Beenker, G. J. F. Van Son, H. Begthel, G. D. Amatngalim, J. M. Beekman, H. Clevers, J. Den Hertog, Dual RNA sequencing of a co-culture model of Pseudomonas aeruginosa and human 2D upper airway organoids. *Sci Rep* **15**, 2222 (2025).

37. S. Bouheraoua, S. Cleeves, M. Preusse, M. Müsken, P. Braubach, M. Fuchs, C. Falk, K. Sewald, S. Häussler, Establishment and characterization of persistent *Pseudomonas aeruginosa* infections in air–liquid interface cultures of human airway epithelial cells. *Infect Immun* **93**, e00603-24 (2025).

38. P. Laborda, S. Lolle, S. Hernando-Amado, M. Alcalde-Rico, K. Aanæs, J. L. Martínez, S. Molin, H. K. Johansen, Mutations in the efflux pump regulator MexZ shift tissue colonization by Pseudomonas aeruginosa to a state of antibiotic tolerance. *Nat Commun* **15**, 2584 (2024).

39. M. S. Walters, K. Gomi, B. Ashbridge, M. A. S. Moore, V. Arbelaez, J. Heldrich, B.-S. Ding, S. Rafii, M. R. Staudt, R. G. Crystal, Generation of a human airway epithelium derived basal cell line with multipotent differentiation capacity. *Respir Res* **14**, 135 (2013).

40. A. Espaillat, C. A. Colque, D. Rago, R. La Rosa, S. Molin, H. K. Johansen, Adaptive Evolution of *Pseudomonas aeruginosa* in Human Airways Shows Phenotypic Convergence Despite Diverse Patterns of Genomic Changes. *Molecular Biology and Evolution* **41**, msae022 (2024).

41. R. L. Marvig, L. M. Sommer, S. Molin, H. K. Johansen, Convergent evolution and adaptation of Pseudomonas aeruginosa within patients with cystic fibrosis. *Nat Genet* **47**, 57–64 (2015).

42. D. Balasubramanian, L. Schneper, H. Kumari, K. Mathee, A dynamic and intricate regulatory network determines Pseudomonas aeruginosa virulence. *Nucleic Acids Research* **41**, 1–20 (2013).

43. A. Brencic, S. Lory, Determination of the regulon and identification of novel mRNA targets of *Pseudomonas aeruginosa* RsmA. *Molecular Microbiology* **72**, 612–632 (2009).

44. J. A. Bartell, L. M. Sommer, J. A. J. Haagensen, A. Loch, R. Espinosa, S. Molin, H. K. Johansen, Evolutionary highways to persistent bacterial infection. *Nat Commun* **10**, 629 (2019).

45. N. Cramer, J. Klockgether, B. Tümmler, Microevolution of Pseudomonas aeruginosa in the airways of people with cystic fibrosis. *Current Opinion in Immunology* **83**, 102328 (2023).

46. C. R. Armbruster, C. W. Marshall, A. I. Garber, J. A. Melvin, A. C. Zemke, J. Moore, P. F. Zamora, K. Li, I. L. Fritz, C. D. Manko, M. L. Weaver, J. R. Gaston, A. Morris, B. Methé, W. H. DePas, S. E. Lee, V. S. Cooper, J. M. Bomberger, Adaptation and genomic erosion in fragmented Pseudomonas aeruginosa populations in the sinuses of people with cystic fibrosis. *Cell Reports* **37**, 109829 (2021).

47. E. Pesce, E. Sondo, L. Ferrera, V. Tomati, E. Caci, P. Scudieri, I. Musante, M. Renda, N. Baatallah, N. Servel, A. Hinzpeter, D. di Bernardo, N. Pedemonte, L. J. V. Galietta, The Autophagy Inhibitor Spautin-1 Antagonizes Rescue of Mutant CFTR Through an Autophagy-Independent and USP13-Mediated Mechanism. *Front. Pharmacol.* **9**, 1464 (2018).

48. N. Pedemonte, F. Bertozzi, E. Caci, F. Sorana, P. Di Fruscia, V. Tomati, L. Ferrera, A. Rodríguez-Gimeno, F. Berti, E. Pesce, E. Sondo, A. Gianotti, P. Scudieri, T. Bandiera, L. J. V. Galietta, Discovery of a picomolar potency pharmacological corrector of the mutant CFTR chloride channel. *Sci. Adv.* **6**, eaay9669 (2020).

49. A. Gianotti, L. Delpiano, E. Caci, In vitro Methods for the Development and Analysis of Human Primary Airway Epithelia. *Front. Pharmacol.* **9**, 1176 (2018).

50. M. F. Moradali, S. Ghods, B. H. A. Rehm, Pseudomonas aeruginosa Lifestyle: A Paradigm for Adaptation, Survival, and Persistence. *Front. Cell. Infect. Microbiol.* **7** (2017).

51. B. Polack, D. Dacheux, I. Delic-Attree, B. Toussaint, P. M. Vignais, ThePseudomonas aeruginosa fumcandsodaGenes Belong to an Iron-Responsive Operon. *Biochemical and Biophysical Research Communications* **226**, 555–560 (1996).

52. H. Arai, Regulation and Function of Versatile Aerobic and Anaerobic Respiratory Metabolism in Pseudomonas aeruginosa. *Front. Microbio.* **2** (2011).

53. X. Shao, C. Yao, Y. Ding, H. Hu, G. Qian, M. He, X. Deng, The transcriptional regulators of virulence for Pseudomonas aeruginosa: Therapeutic opportunity and preventive potential of its clinical infections. *Genes & Diseases* **10**, 2049–2063 (2023).

54. S. Fenn, J.-F. Dubern, C. Cigana, M. De Simone, J. Lazenby, M. Juhas, S. Schwager, I. Bianconi, G. Döring, J. Elmsley, L. Eberl, P. Williams, A. Bragonzi, M. Cámara, NirA Is an Alternative Nitrite Reductase from Pseudomonas aeruginosa with Potential as an Antivirulence Target. *mBio* **12**, e00207-21 (2021).

55. R. Thuenauer, A. Landi, A. Trefzer, S. Altmann, S. Wehrum, T. Eierhoff, B. Diedrich, J. Dengjel, A. Nyström, A. Imberty, W. Römer, The Pseudomonas aeruginosa Lectin LecB Causes Integrin Internalization and Inhibits Epithelial Wound Healing. *mBio* **11**, e03260-19 (2020).

56. L. Camus, F. Vandenesch, K. Moreau, From genotype to phenotype: adaptations of Pseudomonas aeruginosa to the cystic fibrosis environment. *Microbial Genomics* **7** (2021).

57. E. Rossi, M. Falcone, S. Molin, H. K. Johansen, High-resolution in situ transcriptomics of Pseudomonas aeruginosa unveils genotype independent patho-phenotypes in cystic fibrosis lungs. *Nat Commun* **9**, 3459 (2018).

58. P. Losol, M.-H. Ji, J. H. Kim, J.-P. Choi, J.-E. Yun, J.-H. Seo, B.-K. Kim, Y.-S. Chang, S.-H. Kim, Bronchial epithelial cells release inflammatory markers linked to airway inflammation and remodeling in response to TLR5 ligand flagellin. *World Allergy Organization Journal* **16**, 100786 (2023).

59. A. Muggeo, C. Coraux, T. Guillard, Current concepts on Pseudomonas aeruginosa interaction with human airway epithelium. *PLoS Pathog* **19**, e1011221 (2023).

60. I. Jurado-Martín, M. Sainz-Mejías, S. McClean, Pseudomonas aeruginosa: An Audacious Pathogen with an Adaptable Arsenal of Virulence Factors. *IJMS* **22**, 3128 (2021).

61. J. Meisner, J. B. Goldberg, The Escherichia coli *rhaSR-PrhaBAD* Inducible Promoter System Allows Tightly Controlled Gene Expression over a Wide Range in Pseudomonas aeruginosa. *Appl Environ Microbiol* **82**, 6715–6727 (2016).

62. K. L. Palmer, L. M. Aye, M. Whiteley, Nutritional Cues Control *Pseudomonas aeruginosa* Multicellular Behavior in Cystic Fibrosis Sputum. *J Bacteriol* **189**, 8079–8087 (2007).

63. A. J. Westermann, S. A. Gorski, J. Vogel, Dual RNA-seq of pathogen and host. *Nat Rev Microbiol* **10**, 618–630 (2012).

64. E. Rossi, M. Lausen, N. F. Øbro, C. A. Colque, B. U. Nielsen, R. Møller, C. De Gier, A. Hald, M. Skov, T. Pressler, S. R. Ostrowski, H. V. Marquart, H. K. Johansen, Widespread alterations in systemic immune profile are linked to lung function heterogeneity and airway microbes in cystic fibrosis. *Journal of Cystic Fibrosis* **23**, 885–895 (2024).

65. M. I. Love, W. Huber, S. Anders, Moderated estimation of fold change and dispersion for RNA-seq data with DESeq2. *Genome Biol* **15**, 550 (2014).